scientific reports

Check for updates

OPEN

Turbidity and suspended sediment relationship based on sediment composition and particle size distribution

Jongmin Kim[1], Siyoon Kwon[2,3], Sewoong Chung[4] & Young Do Kim[1]✉

High turbidity in rivers, intensified by extreme rainfall associated with climate change, poses a great challenge to water resource management globally. To manage and control turbidity events, prediction models have been developed utilizing suspended sediment (SS) data. However, traditional methods for measuring SS data, such as water sampling and laboratory analysis, are time-consuming and impractical for real-time applications. Although the turbidity–SS relationship is widely used, its accuracy depends on sediment particle size distribution. To address this limitation, we developed turbidity–SS equations adaptive to various SS fractions, using data from controlled circulating flume experiments designed to reflect sediment characteristics of a natural river. The results showed significant improvements in the linear turbidity–SS relationship, with R^2 values ranging from 0.60 to 0.99, depending on sediment fractions. These equations were applied to field data from the area upstream of Soyanggang Dam in South Korea, yielding error rates of 1–18%. This study highlights the importance of incorporating sediment fraction variability into turbidity–SS models, which significantly improves their accuracy and reliability. The proposed approach offers a practical and scalable solution for real-time and large-scale SS monitoring, contributing to improved water quality management in various riverine conditions.

Keywords Turbidity, Suspended sediment, Turbidity–SS relationship, Sediment fractions, Particle size distribution

Turbidity events are triggered by heavy rainfall during the monsoon season and typhoons, resulting in massive influxes of sediment into rivers. This sudden surge in turbidity prevents fine particles from settling, allowing suspended sediments (SS) to be carried downstream to reservoirs where they contribute to prolonged turbidity[1,2]. Concentrated summer rainfall patterns make South Korea particularly susceptible to turbidity issues. Historical typhoons, including Rusa (2002), Maemi (2003), and Ewiniar (2006), caused significant turbidity problems. Despite mitigation efforts by the central government and K-Water, recent high turbidity events in 2020, following the consecutive typhoons Maysak and Haishen, underscore the intensifying impact of climate change on extreme weather events and water quality[3–5]. These events highlight the need to revisit and improve past turbidity management strategies, including those applied in upstream, in-reservoir, and downstream areas. The high prevalence of turbidity in Korea is particularly concerning, given the country's heavy reliance on rivers and reservoirs for water, having implications for agriculture, industry, and aquatic ecosystems[6–8]. Effective management and operation of dams, particularly upstream of reservoirs, based on turbidity distribution is essential for addressing prolonged turbidity issues[9]. To monitor turbidity, national institutions primarily use turbidity and SS concentrations as indicators[10,–13]. Turbidity is easy to measure, and real-time data are available through the national monitoring network; however, turbidity readings can vary substantially depending on particle composition and mineral properties. These variations arise from differences in the spectral characteristics of particles, such as their optical scattering and absorption properties, which influence turbidity measurements[14,15]. As a result, relying solely on turbidity data may lead to inaccuracies, especially during events

[1]Department of Civil and Environmental Engineering, Myongji University, 116 Myeongji-ro, Cheoin-gu, Yongin, Gyeonggi, South Korea. [2]Department of Civil and Environmental Engineering, Seoul National University, 1 Gwanak-ro, Gwanak-gu, Seoul, South Korea. [3]Fariborz Maseeh Department of Civil, Architectural and Environmental Engineering, The University of Texas at Austin, Austin, TX, USA. [4]Department of Environmental Engineering, Chungbuk National University, 1 Chungdae-ro, Seowon-gu, Cheongju, Chungcheongbuk, South Korea. ✉email: ydkim@mju.ac.kr

involving diverse particle compositions. To address this, it is essential to regularly measure SS concentration (SSC) alongside turbidity. This ensures more accurate monitoring and effective management of sediment-related issues. Furthermore, reliable SSC data are essential for robust calibration of turbidity estimation equations, enhancing the precision and reliability of sediment assessments. Korea's national monitoring network records SSCs at key sites on a weekly to monthly basis, while turbidity is measured by K-Water's automated monitoring network at intervals of 10 to 60 min[16]. Turbidity prediction models are widely used to evaluate the occurrence, behavior, and management of turbidity events[17,18]. Accurate turbidity prediction is crucial for evaluating turbidity reduction measures, and active research in this area has been ongoing for decades[19–21].

The key input for turbidity prediction models is SS data, which are currently obtained through sampling and laboratory analysis. However, sampling-based monitoring has limited predictive accuracy due to its low temporal resolution. Conventional turbidity–SS relationships rely on long-term data collection, typically spanning a single season to several years. However, despite the variability in sediment particle size distribution, these relationships are expressed using a single equation without considering such differences. Consequently, even at the same site, changes in particle size distribution over time can alter the turbidity–SS relationship, yet this limitation is not accounted for in conventional approaches.

Data-based flow–SS relationship curves have historically been used to indirectly estimate SS based on flow rate[22]. However, flood-induced changes in riverbed sediment properties and hydraulic characteristics necessitate regular recalibration. Recent research has shown that the turbidity–SS relationship provides higher predictive accuracy resulting in an increased reliance on this method[23].

In turbidity prediction models, such as the Aquatic Ecology Model 3D (AEM3D), particle concentration is estimated based on particle size fractions. This approach suggests that turbidity–SS relationships vary depending on the prevalence of fine particles, prompting research into associated variables[24–28]. Given that the accuracy of these relationships may decrease due to factors such as rainfall events and field conditions, calculating the fractions of particle types (i.e., clay, silt, and sand) more precisely could improve accuracy. For more accurate SS monitoring, an increasing number of studies utilize sensor-based measurements with the laser in-situ scattering and transmissometry (LISST) sensor (e.g., LISST-200X, Sequoia Scientific, Inc., USA)[29,30]. Common research methods include calibration techniques, SSC calculations based on particle size, SSC calculations from sampling and laboratory analysis, and the application of particle size distribution calculations[31–33]. However, field monitoring to improve turbidity–SS relationships is highly sensitive to rainfall events and onsite conditions, resulting in widely fluctuating error rates. This variability limits the applicability of sediment fraction and concentration measurements, making it challenging to generalize LISST sensor data for accurate concentration estimation[34]. These approaches also do not fully account for variations in sediment composition, particularly differences in particle size distribution. To address this limitation, this study aimed to enhance existing turbidity–SS relationship models by incorporating sediment particle size distribution. By considering variations in sediment fractions, including clay, silt, and sand, the study enhances the accuracy of turbidity-based SS estimations and improves the reliability of predictive models.

Specifically, this study examined particle fractions measured using the LISST-200X at an upstream site of Soyang Lake in Inje, South Korea, a location with a history of turbidity issues[35]. A controlled laboratory setup was designed to collect turbidity and corresponding sediment data from artificial particle samples, with specific fractions and concentrations based on LISST-200X measurements. These samples were circulated in an indoor recirculating flume to simulate sediment-laden water conditions. Additionally, an upgraded LISST-200X, paired with a YSI-EXO sensor (YSI, Inc., USA) was used to simultaneously measure turbidity, SS, and particle size distribution for improved turbidity monitoring. The primary goal of this study was to establish turbidity–SS relationships based on particle fraction compositions and validate these relationships under field conditions to improve the accuracy and applicability of turbidity–SS models. The findings contribute to enhancing the precision and efficiency of turbidity-based SS estimation by accounting for the influence of rainfall events on turbidity characteristics and changes in material properties.

Results

To ensure reliable data acquisition in the flume, we obtained turbidity and SSC measurements under controlled conditions. For each experimental case, we continuously collected data at 1 Hz for approximately 3 min after stabilizing both velocity and water level. The time-averaged values were then used for analysis.

To assess the uncertainty introduced by turbulence and evaluate the stability of SSC measurements, we visualized the data variation using boxplots for each SSC case (Fig. 1). The results revealed a progressive increase in SSC across the experimental cases, accompanied by relatively minor variability at lower SSC levels. Although measurement variability tended to increase at higher SSC levels, indicated by wider interquartile ranges (IQR) and more frequent outliers, the overall trends remained clear and consistent. This consistency implies that turbulence had a negligible impact on the measured data under the controlled conditions employed in our experiments. In general, cohesive sediments are susceptible to flocculation influenced by turbulence; however, within the concentration range examined in this study, such turbulence-driven effects were not significant enough to notably affect SSC measurement stability. Furthermore, by utilizing time-averaged values, turbulence-induced fluctuations were effectively minimized, ensuring a robust and reliable dataset for subsequent analysis.

Moreover, to evaluate the impact of flow velocity on the turbidity–SSC relationship, we conducted measurements across velocities ranging from 0.12 to 0.42 m/s, in increments of 0.1 m/s (Fig. 2). Linear regression analyses revealed minimal changes in the turbidity–SSC relationships as velocity increased, indicating that variations due to flow velocity were negligible. In contrast, significant differences in the regression slopes were observed across cases with varying particle size fractions (clay, silt, and sand). These results suggest that particle size distribution had a greater influence on the turbidity–SSC relationship than velocity did. Therefore, for subsequent experiments, we fixed the velocity at 0.42 m/s—a representative velocity during typical flood

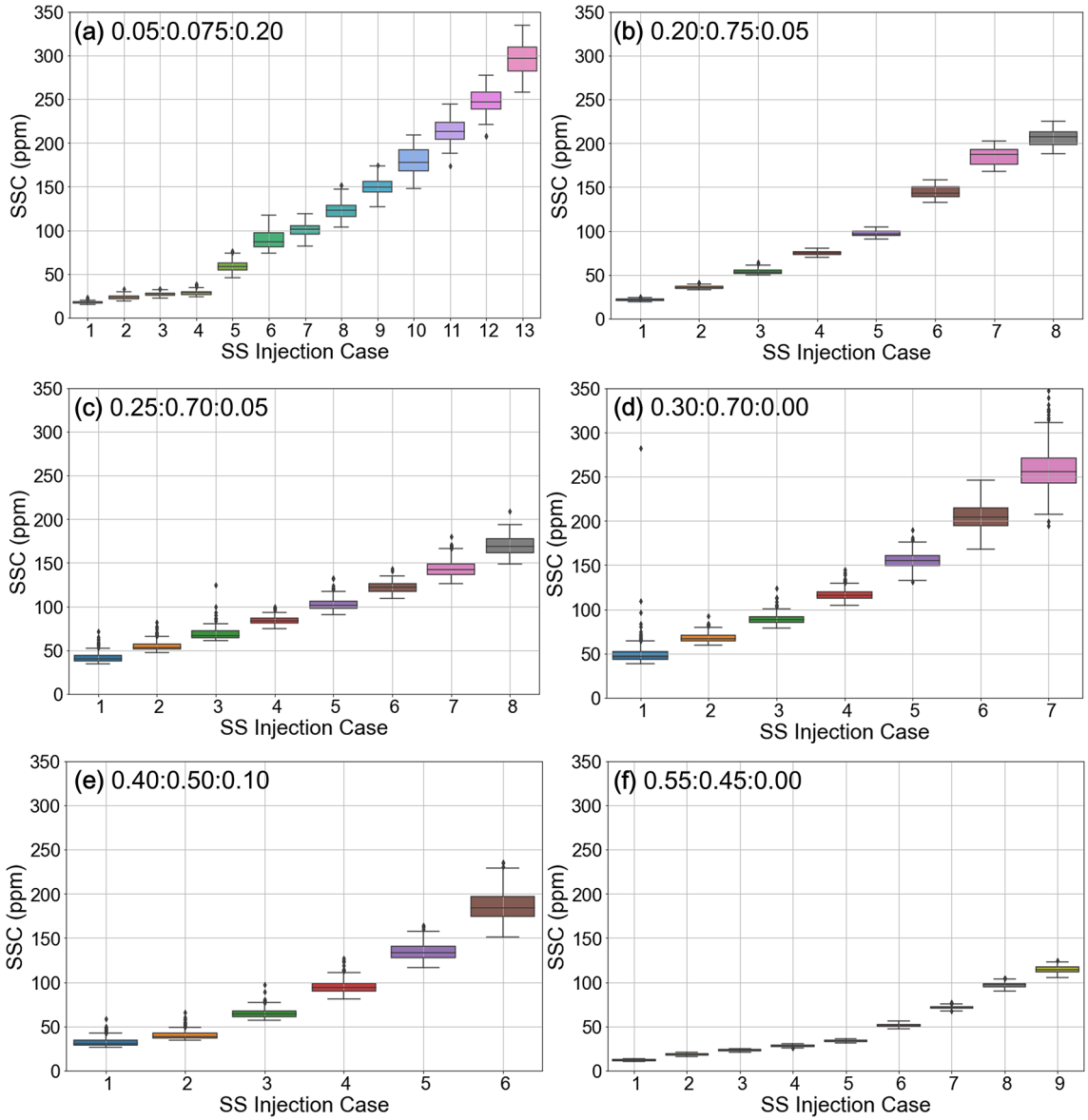

Fig. 1. Temporal variability of SSC measurements across experimental cases. The numbers above each case indicate the fraction of clay, silt, and sand, respectively.

conditions—to systematically investigate the effects of sediment fractions on the turbidity–SSC relationship while minimizing velocity-induced uncertainties.

To evaluate the impact of particle size on the turbidity–SS relationship, we conducted a preliminary experiment with samples classified by particle size using 400 (< 38 μm), 100 (75–150 μm), and 60 (150–250 μm) mesh sieves with corresponding clay: silt: sand fractions of 0.21:0.66:0.13, 0.12:0.81:0.08, and 0.06:0.57:0.37, respectively (Fig. 3a–c). The turbidity–SS relationship was developed using linear regression, as shown in Fig. 3d.

The turbidity–SS regression equation for the smallest sample, collected with a 400-mesh sieve, is represented by Eq. (1), with a coefficient of determination (R^2 of 0.99. Equation (2) and (3) correspond to larger fractions (100-mesh and 60-mesh, respectively), with R^2 values of 0.93 and 0.86.

$$y = 0.513x - 2.064 \tag{1}$$

$$y = 0.351x + 1.708 \tag{2}$$

$$y = 0.284x - 1.733 \tag{3}$$

Figure 3d shows that the relationship between SSC and turbidity is stronger for smaller particle sizes. For larger particles, however, greater irregularity and variability in concentration measurements—caused by particle movement and settling within the LISST-200X's optical path—resulted in larger concentration deviations compared to smaller particles. Additionally, the trend slope of the relationship is steeper for smaller particles,

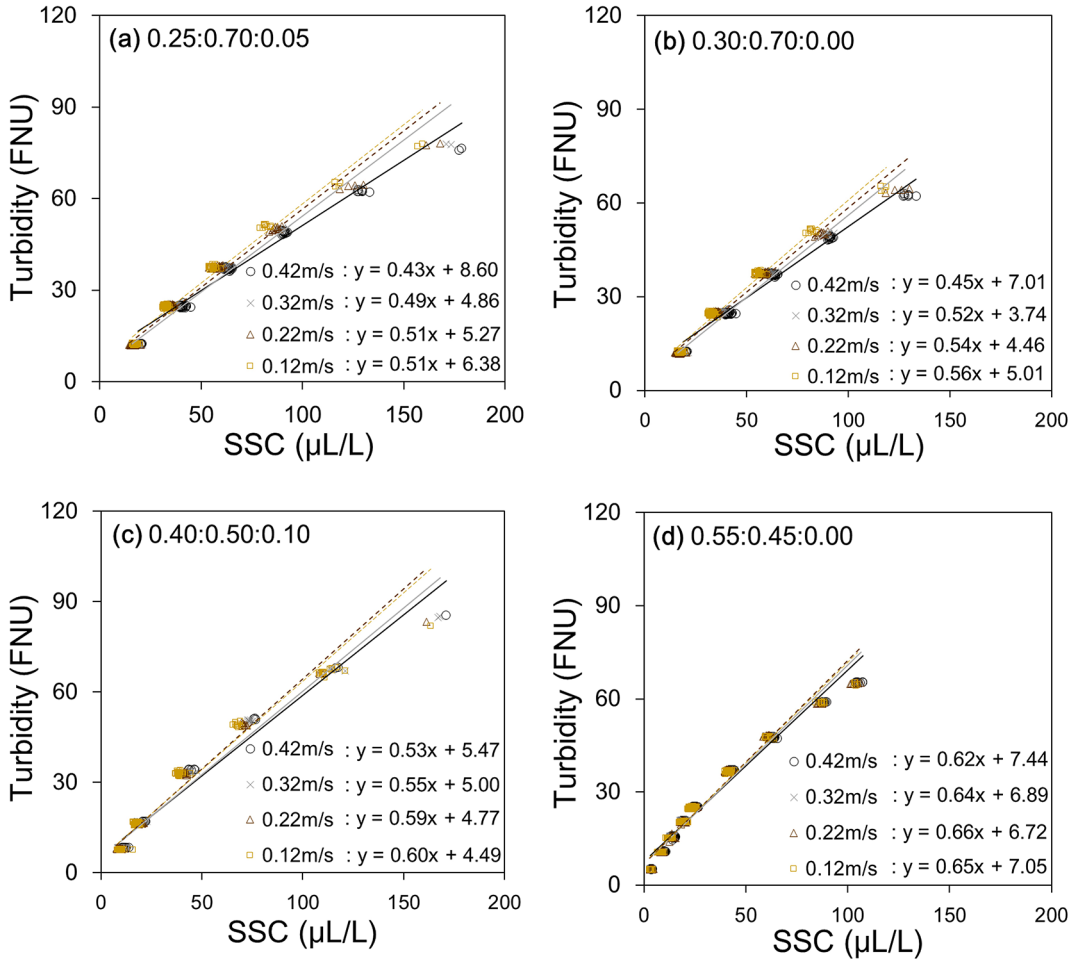

Fig. 2. Sensitivity of turbidity–SSC relationships to flow velocity under different sediment Fraction compositions.

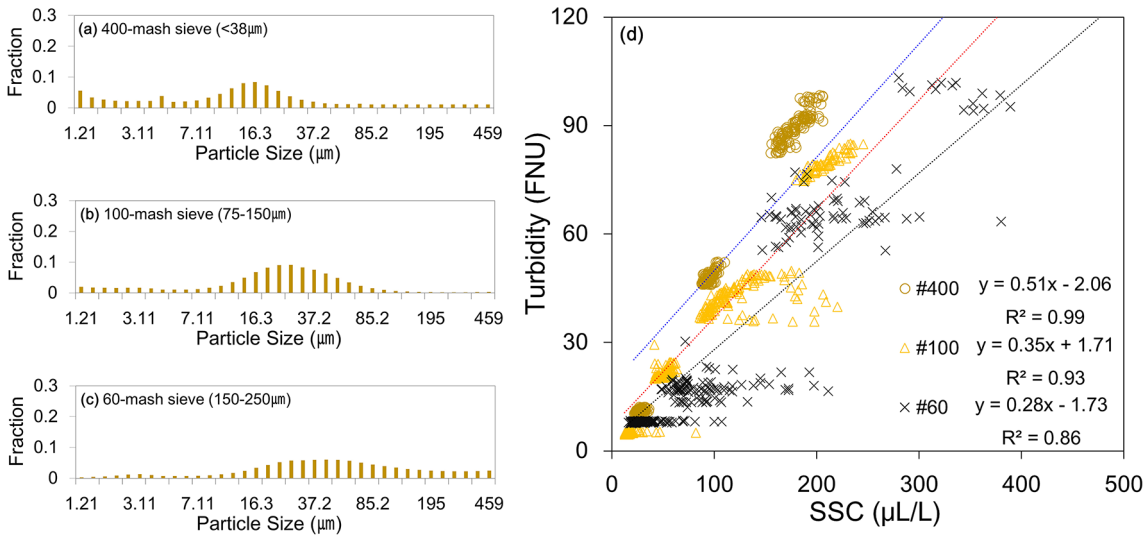

Fig. 3. Particle size distribution of sediment samples used in the experiments: (**a**) 400-mesh sieve (< 38 μm), (**b**) 100-mesh sieve (75–150 μm), and (**c**) 60-mesh sieve (150–250 μm). (**d**) Variation in the turbidity-suspended sediment relationship with particle size (shaking sieve machine).

suggesting that at the same concentration, smaller particles scatter light more effectively than larger particles and thus have a greater impact on turbidity. This result highlights the importance of particle size and fraction in the turbidity–SS relationship.

Figure 4 presents the particle fractions and particle size distributions of samples measured at 1-s intervals over 3 min for each case. The experimental results showed that silt had the highest proportion overall. It was observed that as the proportion of clay increased, the maximum measured concentration decreased. This is because the measurements were taken up to the multiple scattering threshold using LISST-200X, indicating that as the proportion of clay increased, the concentration at which multiple scattering occurred became lower.

Figure 5a presents the turbidity–SS relationships for all six cases prior to classification based on particle size fraction. The relationship appears generally linear, with a slope of 0.297 and a y-intercept of 7.892. However, the R^2 value of 0.602, indicating a relatively weak correlation, suggests that the derived equation may not be suitable for practical applications. The scattered distribution seen in Fig. 5a likely results from variations in sediment particle size, optical scattering effects, and differences in particle settling behavior as they pass through the LISST-200X optical path. This suggests that applying a single turbidity–SS equation to all cases may not adequately capture the relationship due to the inherent variability in sediment fraction composition.

By segmenting the dataset based on particle size fractions, the influence of sediment composition on turbidity–SS relationships became more apparent. The scattered data distribution in Fig. 5a indicates that a fraction-specific approach is necessary to reduce variability and improve predictability. The results confirm that a general turbidity–SS equation without fraction classification may not be reliable, whereas distinguishing cases based on particle fraction significantly enhances linearity. This classification method provides a strong basis for refining turbidity-based SS estimation models, particularly in studies utilizing LISST-200X.

The R^2 value for each fraction-based sample ranged between 0.900 and 0.976, demonstrating high accuracy (Fig. 5b). However, except for the 0.55:0.45:0.00 case, there was considerable variation in SS data across the different concentrations. To address this, a median filter and time-averaging technique were applied to the data, as shown in Fig. 5c, d.

The median filter effectively reduced the high variability in the SS data by focusing on outlier removal and emphasizing the central values, as shown in Fig. 5c. While the 0.55:0.45:0.00 case already exhibited high accuracy, the R^2 for other cases also showed slight improvements. Figure 5d shows the results of sequential time-averaging, where the optimal averaging time for each concentration level was determined based on standard deviation and an allowable error rate. This approach yielded results comparable to or slightly better than those obtained with the median filter, with improvements observed in concentration-dependent SS variability compared to Fig. 5c. Thus, the time-averaging method proved more effective at accounting for SS data variability than a simple median value adjustment, confirming this technique as an optimal correction method.

Figure 5d confirms that the turbidity–SS relationship following time-averaged correction tended toward turbidity for smaller particle sizes. High R^2 values ranging from 0.959 to 0.989 were observed for each particle size fraction. In all cases, other than the 0.05:0.75:0.20 case, a decrease in SSC was observed at the maximum measured concentration, likely due to multiple scattering effects caused by high turbidity near the LISST-200X's maximum concentration limit, leading to overestimation.

The applicability of the derived turbidity–SS relationship was assessed using field data collected from the upstream area of Soyang Lake. Field data were gathered during rainfall events, with measurements taken once

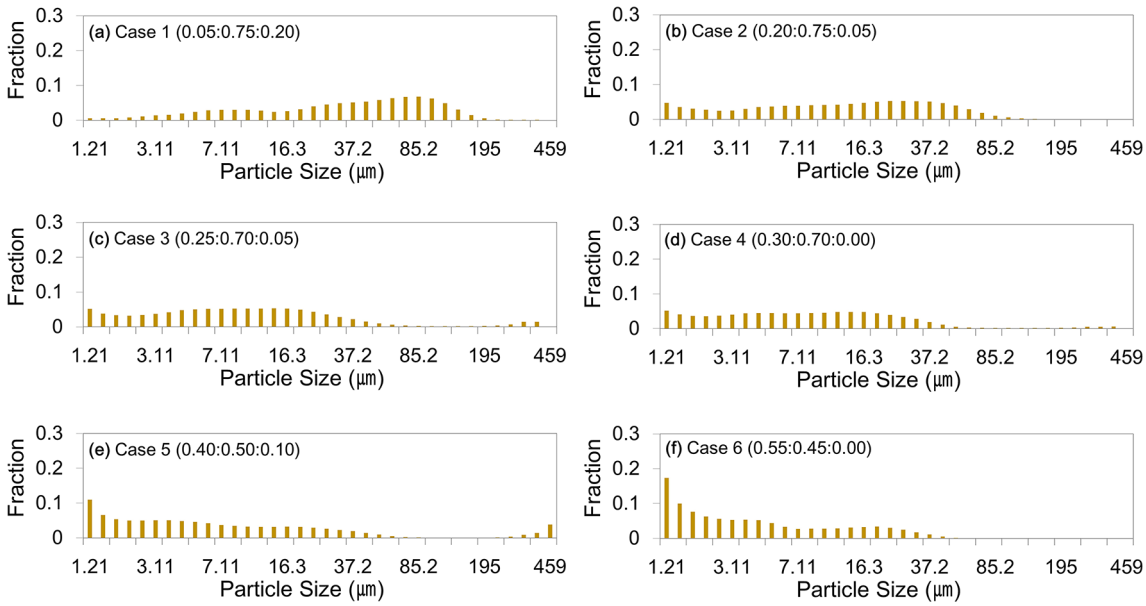

Fig. 4. Distribution of particle size measured using a LISST-200X device for each case of clay: silt: sand ratio: (**a**) case 1 (0.05:0.75:0.20); (**b**) case 2 (0.20:0.75:0.05); (**c**) case 3 (0.25:0.70:0.05); (**d**) case 4 (0.30:0.70:0.00); (**e**) case 5 (0.40:0.50:0.10); (**f**) case 6 (0.55:0.45:0.00).

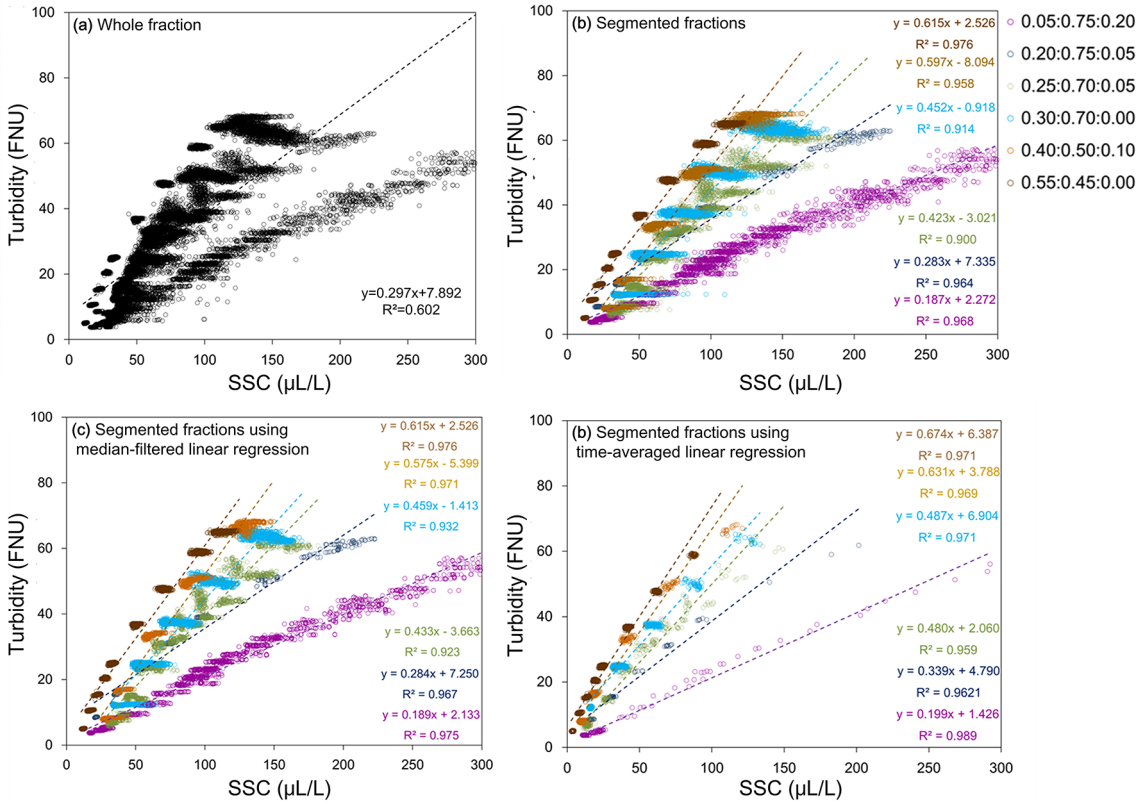

Fig. 5. Relationship between turbidity and suspended sediment concentration (SSC): (**a**) whole fraction; (**b**) segmented fractions; (**c**) segmented fractions using median-filtered linear regression; (**d**) segmented fractions using time-averaged linear regression.

Time	Water level (m)	Flow rate (m^3/s)	Turbidity (FNU)	LISST measured fraction	SSC (μL/L)	Used equation	Estimated turbidity	Actual turbidity	Error rate
06.29.2022 15:30	2.76	209.24	95.30	0.20:0.60:0.20	273.5	y = 0.339x + 4.790	97.5	95.3	0.02
07.17.2024 17:35	3.25	389.78	77.63	0.10:0.60:0.30	311.8	y = 0.199x + 1.426	63.5	77.6	0.18
07.17.2024 08:00	2.98	295.79	16.42	0.00:0.70:0.30	66.0	y = 0.199x + 1.426	14.6	16.0	0.09
07.18.2024 09:40	3.14	351.22	18.58	0.00:0.70:0.30	73.2	y = 0.199x + 1.426	16.0	18.6	0.14
07.18.2024 11:50	3.33	419.18	53.99	0.00:0.70:0.30	262.1	y = 0.199x + 1.426	53.59	54.0	0.01

Table 1. Field data from the upstream area of Soyang lake in Inje, Gangwon-do, Korea, and validation results of turbidity-SS relationship equations applied to the field data. *SSC* suspended sediment concentration.

on June 29, 2022, and eleven times on July 17 and 18, 2024. Measurements covered one flow recession event and ten flow rising events following rainfall (Table 1).

Due to high turbidity on July 18, 2024, field measurements taken from 11:50 a.m. onward exceeded the LISST-200X's measurable concentration range. Consequently, the derived equations were validated using the five applicable datasets. The relationship equations, adjusted to match particle fraction conditions similar to the experimental cases, are presented in Table 1. The equations derived from Case 1 (0.05:0.75:0.20) and Case 2 (0.20:0.74:0.10) in Table 1 were used as the relationship equation. The error rate ranged from 0.01 to 0.18. The 0.00:0.70:0.30 fraction, which closely matched Case 1, showed relatively high accuracy, while the 0.20:0.60:0.20 fraction, similar to Case 2, also demonstrated high accuracy with an error rate of 0.02.

Discussion

This study aimed to improve the turbidity–suspended sediment (SS) relationship by incorporating sediment fraction variability into the model. To achieve this, turbidity monitoring was conducted during extreme events, but field data were collected for only three days (once on June 29, 2022, and eleven times on July 17–18, 2024). This limited field validation makes it difficult to fully account for seasonal variability. However, applying the improved relationship derived from the collected data resulted in an error rate ranging from 0.02 to 0.18, and the applicability of the relationship was found to be high, particularly in cases with similar sediment fractions.

Although the experimental setup differs from open boundary conditions in natural rivers, it was designed to analyze the influence of sediment fraction variability on turbidity measurements rather than replicate real sediment transport processes. Since turbidity–SS relationships can vary depending on the particle size distribution formed under different conditions, considering sediment fraction compositions plays a crucial role in improving the accuracy of turbidity-based SS estimation.

One of the key challenges in turbidity–SS estimation is the temporal variation in sediment particle size distribution due to hydrodynamic and geomorphological changes, which is particularly pronounced during flood events. As shown in Fig. S1, particle size distribution varied significantly across different measurement periods, indicating the need for site-specific calibration that considers changes in sediment fractions due to seasonal and rainfall events. Conventional turbidity–SS relationships often assume a constant composition of suspended sediment, which may lead to reduced accuracy when applied under various temporal and hydrological conditions. This study confirmed that incorporating sediment fraction data improves estimation accuracy, but long-term field monitoring under diverse hydrological conditions is necessary to validate the reliability of the proposed methodology.

Beyond sediment fraction and particle size distribution, other environmental factors, including flow velocity, water temperature, organic matter content, and pH—can influence turbidity events and suspended sediment transport. Flow velocity determines the resuspension and settling behavior of particles, impacting turbidity variability under different hydraulic conditions. Water temperature affects sediment flocculation and aggregation, altering the optical properties of suspended particles. Organic matter content may introduce additional variability in turbidity measurements, as organic material can interfere with sensor performance by affecting light scattering and absorption properties. Additionally, pH influences sediment surface charge and aggregation behavior, which can further modify the turbidity–SS relationship. While this study primarily focused on sediment fraction variability, these additional factors warrant further investigation in future studies to improve the robustness of turbidity-based SS estimation models.

Additionally, since most of this study was conducted in a controlled recirculating flume, further field monitoring and application studies are required to generalize the findings to real turbidity events in natural river environments. Expanding field data collection will allow for the development of a more refined turbidity–SS relationship by incorporating a wider range of flow conditions and seasonal variations. Future work could also consider integrating hydrological and biogeochemical factors to better represent the complexity of natural riverine environments.

To address the limitations of optical sensors in high-turbidity conditions, we plan to utilize the LISST-200X Path Reduction Module (PRM), which reduces the optical path length and enables measurements at higher suspended sediment concentrations. This enhancement will allow future studies to extend the measurement range during extreme turbidity events.

Future research should focus on expanding field observations to analyze the temporal variations in turbidity–SS relationships due to seasonal and rainfall effects. Furthermore, integrating real-time monitoring techniques using optical and acoustic sensors with data assimilation methods will enhance the accuracy of turbidity-based SS estimation in natural riverine environments. A more comprehensive approach, incorporating variables such as flow velocity, water chemistry, and organic matter effects, will further improve the reliability of turbidity–SS relationships under varying environmental conditions.

Conclusion

This study experimentally established equations expressing the relationship between turbidity and SS based on particle fraction composition to improve the equations commonly used in analyzing and predicting turbidity events. A sensor-based turbidity monitoring system with improved temporal resolution was employed to derive the relationship equations, addressing the limitations of traditional SS measurement methods. Due to the inability to control particle size fractions in the field, experiments were conducted using commercially available samples in a recirculating flume. Because the laser diffraction-based LISST-200X sensor experiences multiple scattering at turbidity levels with transmission rates below 0.1, the experimental setup was designed within the device's measurable concentration range. Field application of the derived equations confirmed the feasibility of turbidity–SS relationships based on fraction composition and particle size. The main findings of this study are summarized as follows:

(1) Commercially available loess (red clay) was sieved to obtain samples with three particle size ranges: < 38 μm, 75–150 μm, and 150–250 μm. The turbidity–SS relationship was analyzed for each particle size by progressively increasing its concentration, with the trend indicating higher turbidity for smaller particles. This shows that the turbidity–SS relationship varies with particle size. Additional samples with particle sizes ≤ 0.005 mm, ≤ 0.045 mm, and 0.125–0.180 mm were used to create six cases of fraction composition, which were measured for turbidity and SS in the recirculating flume. Although some variation in the fractions occurred during recirculation, the analysis was conducted based on the measured fractions. As the experimental results showed discrepancies in the fractions of the prepared samples and the measurement results, an analysis was conducted based on the measured fractions. Comparing the conventional turbidity–SS relationship calculated from the entire dataset with case-specific turbidity–SS relationships, the case-specific approach displayed a much clearer linear trend than the traditional all-data method.

(2) Linear regression analysis of each case showed that SSCs were more widely distributed relative to turbidity. This SSC variability likely resulted from the continuous movement and settling of particles passing through the LISST-200X optical path, causing concentration fluctuations. Two correction methods were compared to address this variability, a median filter and a time-averaging technique. The comparison confirmed the effectiveness of both methods in reducing data variability and enhancing relationship linearity; however,

time-averaging was more suitable, as it better accounts for SS variability. Consequently, the time-averaging method is favored for its high applicability to linear relationships considering SS–specific variability.

(3) Analysis of the six fraction cases with three experimentally derived particle sizes showed that SSCs exceeded the maximum measurable range of the LISST-200X, resulting in overestimation due to multiple scattering at high turbidity levels. These six estimated fraction cases were validated using field data from the upstream area of Soyang Lake. Although the field data were limited due to high turbidity, the results demonstrated relatively high accuracy, indicating that the derived equations are suitable for practical use.

Methods and materials

Experimental design

Figure 6a shows the specifications and schematic diagram of the recirculating flume used in the experiments. This system consists of a water tank, pump, and settling basin. When a prepared sample is added to the water tank, water is circulated to the settling basin via the pump and then flows back into the water tank, creating a continuous recirculating loop. The flume specifications are as follows: flume dimensions (length × width × height) = 12 × 0.3 × 0.3 m; water tank dimensions (width × length × height) = 2.5 × 2.5 × 1.2 m; flume gradient (S) = 0.0175 (1.75%); maximum flow rate = 0.42 m/s; and water level = 20 cm, maintained at a constant level with a tail gate.

A preliminary experiment was conducted to investigate how variations in particle size fractions influence turbidity–SS relationships. Commercially available loess (red clay) was used as the sample material, processed through a series of stacked sieves with different mesh sizes (60, 100 and 400) to separate particles by size (Fig. 6b). The sample material was subjected to vibration for 15 min using a shaking sieve machine. Particles were then classified by size, collecting those remaining on the 400- (< 38 μm), 100- (75–150 μm), and 60-mesh (150–250 μm) sieves for concentration measurements (Fig. 6c).

According to the Unified Soil Classification System (USCS), soil is classified into fine-grained and coarse-grained categories based on particle size and physical properties. The particle size ranges are defined as follows: clay (< 0.005 mm), silt (0.005–0.075 mm), and sand (0.075–4.75 mm). Beyond particle size, the USCS also considers physical properties, such as the plasticity index and liquid limit, to define the engineering characteristics of soil. This study aimed to establish a relationship between turbidity and SSC based on particle size distribution measured with the LISST-200X sensor, using clay, silt, and sand as size-based categories. Due to limitations in preparing particle samples that meet specific particle-size and flume-input quantity requirements, commercially available sieved samples (clay, silt, and sand) were purchased. The particle sizes and corresponding mesh sizes for each material were as follows: clay (< 0.005 mm, 3000 mesh), silt (< 0.045 mm, 325 mesh), and sand (0.125–0.180 mm, 80 and 120 mesh). For each particle size fraction, data from turbidity events recorded at the upstream area of Soyang Lake in Inje, Gangwon-do, during a high turbidity event in August 2022 were used to build six cases with different particle type fractions, which were then introduced into the water tank (Table 2).

Turbidity and SS measurement

To measure SSC and turbidity for each particle size fraction in the recirculating flume, the LISST-200X, which enables particle size distribution and concentration measurements, and the YSI-EXO, a widely used field turbidity sensor, were utilized (Table S1). The LISST-200X was specifically chosen as the research team had previously conducted validation studies comparing it with the hydrometer method[36]. The particle size distributions (PSD) measured by both methods showed similar results, confirming the reliability of the LISST-200X data. To maintain a consistent flow velocity of 0.42 m/s in the flume, flow velocity was measured using a Micro ADV (Nortek, side-looking). The measurement points for turbidity and SS were positioned at the 6 m mark along the flume. The sensors were placed at a height of 7 to 10 cm above the flume bottom to minimize interference from water depth, flow velocity, hydraulic jumps, and potential outliers (Fig. 6d).

To ensure the accuracy and reproducibility of LISST-200X measurements, specific steps were taken to control the distribution of flocculated particles. Prior to each measurement, samples were thoroughly pre-mixed in the water tank to achieve a uniform distribution, minimizing initial aggregation or unintentional segregation. This step minimized the variability in measurements caused by uneven particle dispersion and turbulence. Data was collected at 1-s intervals for a duration of at least 3 min per measurement case. To further enhance the stability of the data, the first 30 s of measurement were excluded to account for initial stabilization. Additionally, measurements were conducted under four different velocity conditions to assess the effect of flow velocity on SSC and turbidity.

Water was supplied to a height of 50 cm in the water tank, and the sample volume was calculated based on particle type and tank volume. Measurements were taken across different concentrations to establish a linear relationship: Cases 1–3 were prepared at 50 mg/L each, and Cases 5–6 with 25 mg/L each, up to the maximum concentration measurable by the LISST-200X (Table 2). Since the LISST-200X measures concentration based on laser scattering and transmission, its measurable range varies with particle size (Table S2). When the SSC exceeds the maximum limit, transmission rates decrease, and below a transmission rate of 0.1, multiple scattering can occur, potentially leading to overestimation of particle size and concentration. To prevent outliers, the water tank was thoroughly cleaned to remove any residual particles between each case. To further minimize the effects of air bubbles and residual particles, measurements for each case were conducted under clean water circulation conditions, with each case serving as a baseline.

Calculation method for turbidity–SS relationship

In expressing the relationship between turbidity and SS, preprocessing is required due to data variation caused by the continuous movement of particles. To address this, the particle size distribution measured under clean water

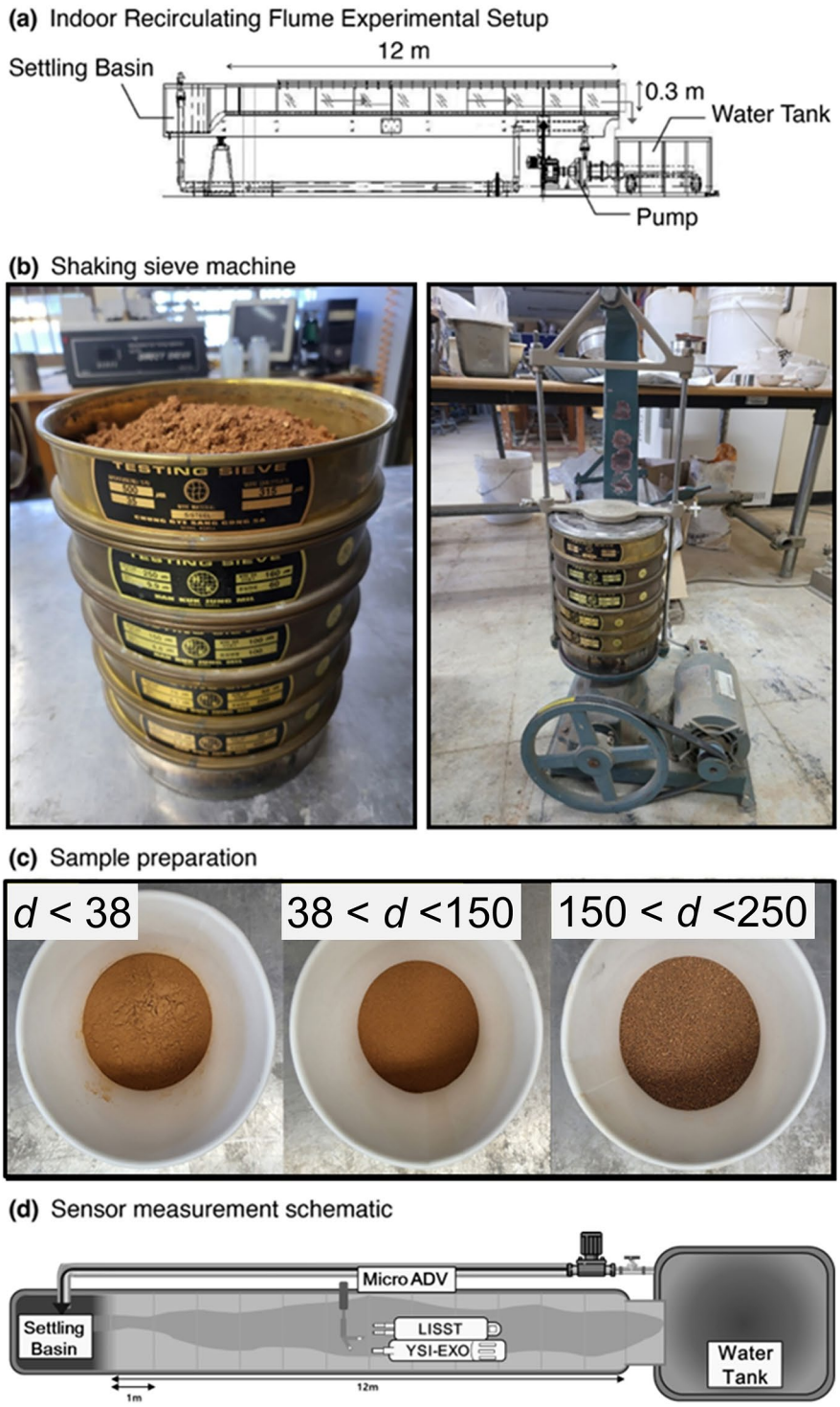

Fig. 6. Experimental setup and sample preparation: (**a**) indoor recirculating flume experimental setup; (**b**) shaking sieve machine; (**c**) sample preparation; (**d**) sensor measurement schematic.

conditions (Base case) was subtracted from the concentration-specific data to obtain the net SS concentration at each concentration level (Eq. 4):

$$Object_{SS1-SS36} = Concentration_{SS1-SS36} - Base_{SS1-SS36} \quad (4)$$

where $Object_{SS1-SS36}$ represents the pure size bin concentrations of SS for each concentration level excluding the influence of clear water; $Concentration_{SS1-SS36}$ denotes the size bin concentrations measured by the LISST-200X

Time	Case	Volume (m^3)	Fraction			Sample weight for 50 mg/L dosage (g)		
			Clay	Silt	Sand	Clay	Silt	Sand
08.09.2022, 14:50	1	3.125	0.00	0.30	0.70	0.00	46.88	109.38
08.09.2022, 21:10	2	3.125	0.10	0.40	0.50	15.63	62.50	78.13
08.09.2022, 22:10	3	3.125	0.20	0.50	0.30	31.25	78.13	43.88
08.10.2022, 00:20	4	3.125	0.30	0.50	0.20	46.88	78.13	31.25
08.10.2022, 02:00	5	3.125	0.40	0.40	0.20	62.50	62.50	31.25
08.10.2022, 02:30	6	3.125	0.60	0.30	0.10	93.75	46.88	15.63

Table 2. Dosage fractions used for turbidity-SS equation selection and the amounts of each sediment type obtained from field monitoring.

for each concentration level; and $Base_{SS1–SS36}$ indicates the size bin concentrations measured by the LISST-200X in clear water conditions.

To obtain a more accurate turbidity–SS relationship equation by accounting for concentration-dependent variability in SS data, smoothing and time-averaging corrections were applied. Smoothing was performed using a median filter, a nonlinear filtering technique that utilizes the median value within a specified range to reduce sharp variations and outliers, thereby mitigating temporary changes and clarifying overall trends. Additionally, time-averaging was applied based on the standard deviation and allowable error rate of SSC variations, calculating a recommended averaging duration and applying it at each specified interval (Eq. 5). The allowable error rate was set at 1%.

$$A_t = (S/e)^2 \tag{5}$$

where A_t represents the length of time to be averaged; S is the standard deviation of the data, indicating the variability of the data; and e is the allowable error rate, representing the specified error limit.

Given the strong linear relationship between turbidity and SS, a linear regression analysis was conducted to derive a straightforward linear equation, facilitating easy interpretation of the relationship between variables. This equation was then applied and validated using data within the LISST-200X measurement range collected at the site upstream of Soyang Lake, as shown in Fig. S2a. Additionally, high turbidity levels were observed, as illustrated in Fig. S2b and S2c. Soyang Lake is a temperate monomictic lake, undergoing one vertical mixing event in winter and forming stratification in summer[37]. The Soyang River is the primary inflow river of Soyang Lake, accounting for more than 90% of its inflow. It spans 60 km in length and has a narrow and elongated topographical characteristic[38]. Additionally, the surrounding areas of the Soyang River and Soyang Lake, including Yanggu-gun, Inje-gun, and Hongcheon-gun, have a high distribution of highland fields. During rainfall events, large amounts of sediment are transported into the river, leading to turbidity issues in the past[39].

Data availability

Processed data supporting the findings of this study are included in the manuscript and its supplementary information files. Additional raw data can be made available upon reasonable request from the corresponding author (ydkim@mju.ac.kr).

Received: 16 January 2025; Accepted: 28 April 2025
Published online: 10 May 2025

References

1. Jansen, F. & Teuling, A. Evaporation from a large lowland reservoir—(dis)agreement between evaporation methods at various timescales. *Hydrol. Earth Syst. Sci. Discuss.* **26**, 1–27 (2019).
2. Kerr, S. J. Silt, turbidity and suspended sediments in the aquatic environment: An annotated bibliography and literature review. *Southern Region Science and Technology Transfer Unit Technical Report TR-008*. https://ontarioriversalliance.ca/wp-content/uploads/2014/07/Silt-Turbidity-and-Suspended-Sediments-in-the-Aquatic-Environment-Marked.pdf (1995).
3. Chung, S. W. & Oh, J. K. River water temperature variations at upstream of Daecheong lake during rainfall events and development of prediction models. *J. Korea Water Resour. Assoc.* **39**, 79–88. https://doi.org/10.3741/JKWRA.2006.39.1.079 (2006).
4. Mouri, G., Shiiba, M., Hori, T. & Oki, T. Modeling reservoir sedimentation associated with an extreme flood and sediment flux in a mountainous granitoid catchment, Japan. *Geomorphology* **125**, 263–270. https://doi.org/10.1016/j.geomorph.2010.09.026 (2011).
5. Palma, P., Ledo, L., Soares, S., Barbosa, I. & Alvarenga, P. Spatial and Temporal variability of the water and sediments quality in the Alqueva reservoir (Guadiana basin; Southern Portugal). *Sci. Total Environ.* **470**, 780–790. https://doi.org/10.1016/j.scitotenv.2013.10.035 (2014).
6. Birmachu, A., Feyissa, T. & Diriba, B. Evaluation of the impacts of turbidity on Gilgel-Gibe I reservoir storage, Omo-Gibe river basin, Ethiopia. *Heliyon* **10**, e36294 (2024).
7. Chung, S. W., Lee, H. S. & Jung, Y. R. Turbidity modeling for a negative buoyant density flow in a reservoir with consideration of multiple particle sizes. *J. Korean Soc. Water Environ.* **24**, 365–377 (2008).
8. Kim, B. C. & Jung, S. M. Turbid storm runoffs in lake Soyang and their environmental effect. *J. Korean Soc. Environ. Eng.* **29**, 1185–1190 (2007).
9. Chung, S. W., Jung, Y. R., Ko, I. H. & Kim, N. I. Development and validation of a decision support system for the real-time monitoring and management of reservoir turbidity flows: A case study for Daecheong dam. *J. Korea Water Resour. Assoc.* **41**, 293–303 (2007).

10. Davies-Colley, R. J. et al. Light attenuation—A more effective basis for the management of fine suspended sediment than mass concentration? *Water Sci. Technol.* **69**, 1867–1874. https://doi.org/10.2166/wst.2014.096 (2014).
11. Davies-Colley, R. & Hughes, A. Sediment-related water quality of small hill-country streams near Whatawhata, new Zealand. Response to integrated catchment management (ICM). *N Z. J. Mar. Freshw. Res.* **54**, 329–353. https://doi.org/10.1080/00288330.2020.1761840 (2020).
12. Davies-Colley, R. J. & Smith, D. G. Turbidity, suspended sediment, and water clarity: A review. *J. Am. Water Resour. Assoc.* **37**, 1085–1101. https://doi.org/10.1111/j.1752-1688.2001.tb03624.x (2001).
13. García, J. T. & Harrington, J. R. Fine sediment modeling during storm-based events in the river Bandon, Ireland. *Water (Switzerland)*. **11**, 1523. https://doi.org/10.3390/w11071523 (2019).
14. Kwon, S., Noh, H., Seo, I. W. & Park, Y. S. Effects of spectral variability due to sediment and bottom characteristics on remote sensing for suspended sediment in shallow rivers. *Sci. Total Environ.* **878**, 163125. https://doi.org/10.1016/j.scitotenv.2023.163125 (2023).
15. Pinet, S., Martinez, J. M., Ouillon, S., Lartiges, B. & Villar, R. E. Variability of apparent and inherent optical properties of sediment-laden waters in large river basins—Lessons from in situ measurements and bio-optical modeling. *Opt. Express*. **25**, A283–A310. https://doi.org/10.1364/oe.25.00a283 (2017).
16. Choi, M., Ryu, J. & Ahn, J. Analysis of the relationship between turbidity and benthic macroinvertebrate communities in the upper stream of Soyang river dam. *J. Korean Soc. Ecol. Infrastruct. Eng.* **32**, 123–135 (2024).
17. Ahn, S. R., Kim, S. H., Yoon, S. W. & Kim, S. J. Evaluation of suspended solids and eutrophication in Chungju lake using CE-QUAL-W2. *J. Korea Water Resour. Assoc.* **46**, 1115–1128 (2013).
18. Hong, J. Y., Jeong, S. K. & Km, B. H. Prediction model suitable for long-term high turbidity events in a reservoir. *J. Korean Soc. Hazard. Mitig.* **21**, 203–213. https://doi.org/10.9798/KOSHAM.2021.21.3.203 (2023).
19. Han, S., Kang, D. K., Shin, H. S., Yu, J. J. & Kim, S. Improvement of suspended solid loads estimation in Nakdong river using minimum variance unbiased estimator. *J. Korean Soc. Water Environ.* **23**, 251–259 (2007).
20. Hoitink et al. Resilience of river deltas in the Anthropocene. *J. Geophys. Res. Earth Surf.* **125**, e2019JF005201 https://doi.org/10.1029/2019jf005201 (2020).
21. Matos, J. P., Hassan, M. A., Lu, X. X. & Franca, M. J. Probabilistic prediction and forecast of daily suspended sediment concentration on the upper Yangtze river. *J. Geophys. Res. Earth Surf.* **123**, 1982–2003. https://doi.org/10.1029/2017JF004240 (2018).
22. Kim, W. G., Jung, K. S. & Yi, Y. K. The variation of water temperature and turbidity of stream flows entering Imha reservoir. *Korean J. Limnol.* **39**, 13–20 (2006).
23. Murillo-Bermúdez, L. F., Salustiano-Martim, A. L. S., Poleto, C. & Dalfré Filho, J. G. Correlation of turbidity and suspended sediment concentration in natural water flow using alternative data of water treatment plant: Case study in the upper jundiaí river, Brazil. *Int. J. River Basin Manag.* **21**, 233–241 (2021).
24. Bright, C. & Mager, S. A national-scale study of spatial variability in the relationship between turbidity and suspended sediment concentration and sediment properties. *River Res. Appl.* **36**, 1449–1459. https://doi.org/10.1002/rra.3679 (2020).
25. Bright, C., Mager, S. & Horton, S. Response of nephelometric turbidity to hydrodynamic particle size of fine suspended sediment. *Int. J. Sediment. Res.* **35**, 444–454. https://doi.org/10.1016/j.ijsrc.2020.03.006 (2020).
26. Landers, M. N. & Sturm, T. W. Hysteresis in suspended sediment to turbidity relations due to changing particle size distributions. *Water Resour. Res.* **49**, 5487–5500 (2013).
27. Lewis, J., Eads, R. & Klein, R. Comparisons of turbidity data collected with different instruments. Report on a cooperative agreement between the California department of forestry and fire protection and USDA forest Service—Pacific Southwest research station #06-CO-11272133-041 (2007).
28. Sehgal, D., Martínez-Carreras, N., Hissler, C., Bense, V. F. & Hoitink, A. J. F. A generic relation between turbidity, suspended particulate matter concentration, and sediment characteristics. *J. Geophys. Res. Earth Surf.* **127**, e2022JF006838. https://doi.org/10.1029/2022JF006838 (2022).
29. Kim, T. W., Kim, Y. D. & Yi, Y. K. A study on field experiment and numerical modeling for efficiency analysis of selective withdrawal in Imha reservoir. *KSCE J. Civ. Eng.* **B32**, 113–121 (2012).
30. Kwak, S. H., Lee, K. S., Cho, H. I., Seo, Y. J. & Lyu, S. W. Field measurement of suspended material distribution at the river confluence. *KSCE J. Civ. Eng.* **37**, 467–474 (2017).
31. Ehrbar, D., Schmocker, L., Vetsch, D. F., Boes, R. M. & Doering, M. Measuring suspended sediments in periglacial reservoirs using water samples, laser in-situ scattering and transmissometry and acoustic doppler current profiler. *Int. J. River Basin Manag.* **15**, 413–431 (2017).
32. Haun, S., Kjæras, H., Løvfall, S. & Olse, N. R. B. Three-dimensional measurements and numerical modeling of suspended sediments in a hydropower reservoir. *J. Hydrol.* **479**, 180–188 (2013).
33. Mikkelsen, O. & Pejrup, M. The use of a LISST-100 laser particle sizer for in-situ estimates of Floc size, density and settling velocity. *Int. J. Mar. Geol.* **20**, 187–195 (2001).
34. Gray, J. R. & Landers, M. N. Measuring suspended sediment. In *Comprehensive Water Quality and Purification* (ed. Ahuja, S.) 157–204 (Elsevier, 2014).
35. Park, H., Chung, S., Cho, E. & Lim, K. Impact of climate change on the persistent turbidity issue of a large dam reservoir in the temperate monsoon region. *Clim. Change* **151**, 365–378 (2018).
36. Kwon, S., Shin, Seo, I. W., Noh, H., Jong, S. H. & You, H. J. Measurement of suspended sediment concentration in open channel flows based on hyperspectral imagery from UAVs. *Adv. Water Resour.* **159**, 104076. https://doi.org/10.1016/j.advwatres.2021.104076 (2021).
37. Kim, Y., Kim, B., Choi, K. & Seo, D. Thermal stratification and density current modeling of Soyang lake using CE-QUAL-W2. *J. Korean Soc. Water Wastewater* **15**, 40–49 (2001).
38. Kim, B. & Jung, S. Turbidity occurrence and its environmental impact in Soyang lake. *J. Korean Soc. Environ. Eng.* **26**, 1185–1190 (2007).
39. Choi, I., Kim, Y. S., Lee, G. C. & Choi, J. NOM characteristics and turbidity in-flow in lake Soyang. *J. Korean Soc. Urban Environ.* **11**, 177–185 (2011).

Acknowledgements

This work is supported by the Korea Environmental Industry & Technology Institute (KEITI) through the Aquatic Ecosystem Conservation Research Program, funded by the Korea Ministry of Environment (MOE) (Grant number 2021003030004).

Author contributions

J.K. collected data, conducted experiments, developed the methodology, and contributed to the manuscript's writing. S.K. contributed to methodology development and participated in the review and editing of the manuscript. S.W.C. was responsible for funding acquisition and project administration. Y.D.K. supervised the study and managed project administration. All authors reviewed and approved the final manuscript.

Declarations

Competing interests
The authors declare no competing interests.

Additional information
Supplementary Information The online version contains supplementary material available at https://doi.org/10.1038/s41598-025-00435-2.

Correspondence and requests for materials should be addressed to Y.D.K.

Reprints and permissions information is available at www.nature.com/reprints.

Publisher's note Springer Nature remains neutral with regard to jurisdictional claims in published maps and institutional affiliations.